16th World Conference on Earthquake Engineering, 16WCEE 2017
Santiago Chile, January 9th to 13th 2017
Paper N° 3481 (Abstract ID)
Registration Code: S-F1464752161

Shear Capacity of 3D Composite Joints of Concrete-Filled Tubular Column

C. Liu[(1)], J. Fan[(2)]

[(1)] PhD. Student, Dept. of Civil Engineering, Tsinghua University, liucheng13@mails.tsinghua.edu.cn
[(2)] Professor, Dept. of Civil Engineering, Tsinghua Univ., fanjsh@tsinghua.edu.cn

Abstract

Shear capacity analysis of the panel zone in a composite joint of concrete-filled steel tubular (CFT) column and steel beam is important for avoidance of premature shear failure of the joint. This paper reviews 2D shear capacity models for joints between CFT column and steel beam. Then a 3D model is proposed for consideration of joints subjected to symmetric beam loadings in two planes and compared to the existing 2D shear capacity models. The effects of encased concrete on the shear capacity of the joint are taken into account for 3D composite joints through an additional compression strut model. A shear force and deformation relationship with four linear segments is thus achieved for a composite joint. To evaluate the corresponding ultimate shear capacity, the modeling results are compared with experiments where specimens fail through shear mode at the joints. It is found that the shear–deformation relationship and ultimate shear capacities predicted for 3D composite joints agree well with the experimental results.

Keywords: 3D CFT joint, bidirectional loading, seismic performance, shear capacity

1. INTRODUCTION

A concrete-filled steel tubular (CFT) column is a structural element in which steel tube and encased concrete carry load by composite action between them. The strength and ductility of the encased concrete is improved by the confinement effect of the steel tube while the local buckling of steel tube is delayed by the encased concrete. Due to advantages such as high strength, excellent ductility and convenience for production and construction, CFT columns are widely used in civil infrastructure. In high-rise buildings, a typical structure system is formed by CFT columns connecting with horizontal structural members (such as beams and floor panels). To ensure structural ductility, premature shear failure of a composite joint should be avoided, especially in structural seismic design. Resistance to earthquake loading in such structural systems depends largely on the capacity of beam-to-column composite joints. Therefore, reliable estimation of the mechanical performance of composite joints between CFT column and beam is essential for structural design.

Extensive experimental and theoretical studies have been performed to understand the performance of the panel zone in a composite joint between CFT column and steel beam and to develop corresponding mechanical models. Analytic formulations for joint shear capacity have also been developed [2~5], but only a 2D configuration (i.e. with CFT column and steel beam in the same plane) has been considered. Research has shown that for a composite joint with internal diaphragms, the steel plates in the joint region and the encased concrete both contribute to the shear capacity of the joint. Using the superposition principle, equations have been formulated to estimate the shear capacity of 2D composite joints by the Architectural Institute of Japan (AIJ) [6]. In the latter research, however, the effects of axial compression on the shear capacity of the panel zone were not considered. Also, it was required that the nominal compression strength of the encased concrete should not be higher than 36 MPa, which largely limited its applicability for high-strength concrete. Koester [1] conducted a series of experiments on split-tee through-bolted moment joints between CFT columns and wide-flange steel beams. In this configuration, the shear capacity of the panel zone of the composite joints was estimated through regression analysis of experimental results without mechanism-based modeling. This limitation therefore restricts the applicability of the proposed shear capacity equation for other forms of composite joints with different connection configurations. Cheng et al. [2,3] proposed an innovative stress-strain model for the panel zone of a composite joint based on the compression strut mechanism, in which the shear force transfer was taken into account through a truss mechanism. The shear capacity formulation developed in this way considered the effects of axial compression on the steel wall and the encased concrete of the column; however, the model became complicated and was not convenient for design purposes. Nishiyama et al. [4] carried out a series of experiments on beam-to-column joints of CFT columns made of high-strength steel and concrete. Their experimental results showed that the design formula given in AIJ (1987) was applicable for unconfined compression strength of concrete up to 110 MPa and tensile strength of steel up to 809 MPa. Similar experiments were conducted by [5] on the joints of high-strength CFT columns and steel beams to investigate structural elastoplastic behavior. A new compression strut mechanism was proposed, where a trilinear shear–deformation relationship was derived for description of the full shear deformation of the panel zone, and the effects of axial force on the behavior of the steel tube were also considered. In that study, the shear deformation at the ultimate strength of the encased concrete was defined as the ultimate shear deformation of the composite joint. Since the ultimate shear strain of concrete is much lower than that of a steel tube, the shear capacity at yielding of the webs of the steel tube was considered in the calculation of the ultimate shear capacity of the joint. In another words, the shear capacity of the joint was provided by the yielding strength of the steel tube plus the ultimate strength of the encased concrete.

Existing formulations of joint shear capacity only consider the shear forces in one plane, corresponding to a 2D composite joint configuration. For realistic composites joints under seismic action, the joint panel zone is actually subjected to shear forces in two planes, corresponding to a 3D joint configuration. For such cases, no mechanical modeling has yet been done to describe joint stiffness and to predict joint shear capacity. In this paper, the 2D load transfer mechanism is extended to a 3D construct to analyze the shear capacity of composite joints in CFT column systems. A 3D load transfer mechanism is analytically modeled and the contributions from both steel column and encased concrete to the shear capacity of the joint panel zone are investigated. In this 3D model, a shear–deformation relationship with four linear segments is considered and its reliability and applicability are verified against previous experimental results including scenarios of composite joints with normal strength concrete [7] and with high-strength concrete [4].

2. ANALYTIC SHEAR CAPACITY MODEL OF A 3D COMPOSITE JOINT

Composite joints in building structures are often under 3D loading conditions, such as those for interior columns, exterior columns and corner columns. In a CFT column system connected by orthogonal beams, the core zone of the 3D composite joint is actually subjected to shear forces from two orthogonal planes, the mechanism of which may be different from that of a planar composite joint. In this section, we establish analytic models of the shear–deformation relationship of steel tube and concrete core. Classical plastic theory is applied to derive the yield and ultimate shear strength of the steel tube. Two forms of strut mechanism are considered to model the ultimate shear capacity of the concrete core. The joint shear–deformation relationship is obtained by the superposition principle, considering the contributions from both steel webs and concrete core. It should be noted that the 3D loading conditions considered in this paper are limited to the scenario where the shear forces from two orthogonal directions are equal (resultant shear force in 45° direction) and the planar shape of the concrete panel is square, since this scenario is the most typical for 3D loading conditions.

2.1 Shear capacity and deformation of steel tube at joint region

The shear capacity of a steel tube at the joint region has two components. One component derives from the shear strength of the webs of the steel tube and the other derives from the shear capacity of the steel tube–inner diaphragm system. In 3D composite joints, the latter component derives mainly from the deformation of the diaphragm system from cubic to parallelepiped shape (similar to a frame mechanism) and it has been reported that this contribution to the total shear capacity of the steel tube at the joint region is very limited [10]. Therefore, only the contribution of the webs to the overall shear capacity of the steel tube is taken into account in this study.

In 3D joint panel zones subjected to shear forces from both *x* and *y* directions, the shear stresses in the webs of the steel tube can be determined by principles of material mechanics. Fig. 1 shows the distributions of shear stresses along the webs of steel tube in the plastic stage (Fig. 1) under bi-directional loading. If $V_x = V_y$, the resultant shear force V acts in a 45° direction to V_x or V_y.

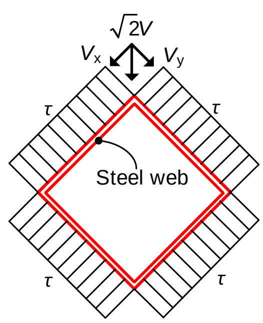

Fig. 1. Distribution of shear stress (τ) of steel webs in plastic stage under bi-directional loading

Assuming a uniform shear stress distribution in the webs of the steel tube in the plastic stage (Fig. 1), the shear stress can then be calculated as:

$$\tau = \frac{V}{A_w} \tag{1}$$

where τ is the shear stress of the webs of the steel tube. According to the von Mises criterion, the yield (τ_y) and maximum (τ_u) shear stress sustained by the webs of the steel tube can be calculated respectively as:

$$\tau_y = \frac{\sqrt{f_{sy}^2 - \sigma_s^2}}{\sqrt{3}} \qquad \tau_u = \frac{\sqrt{f_{su}^2 - \sigma_s^2}}{\sqrt{3}} \tag{2}$$

where f_{sy} and f_{su} are the yielding and ultimate strength of the steel tube respectively and σ_s is the axial compression stress of the steel tube. Hence the yielding (V_{sy}) and ultimate (V_{su}) shear capacities of the webs can be obtained as:

$$V_{sy} = \frac{\tau_y A_w}{k_s} = \frac{A_w\sqrt{f_{sy}^2 - \sigma_s^2}}{\sqrt{3}} \qquad V_{su} = \tau_u A_w = \frac{A_w\sqrt{f_{su}^2 - \sigma_s^2}}{\sqrt{3}} \tag{3}$$

The yielding (γ_{sy}) and ultimate (γ_{su}) shear deformations of the steel tube of a plain joint are given as:

$$\gamma_{sy} = \kappa_s \frac{V_{sy}}{A_w G_s} \tag{4}$$

$$\gamma_{su} = \kappa_s \frac{V_{su} - V_{sy}}{A_w G_s'} + \gamma_{sy} \tag{5}$$

where the shear modulus of the steel tube G_s is normally 79 GPa. G_s' is the slope of the second stage of the trilinear shear–deformation relationship of the steel tube and can be expressed as [5]:

$$G_s' = \frac{1}{\frac{1}{G_s} + \frac{9}{\alpha_s E_s \left(\sigma_s^2 / \tau'^2 + 3\right)}} \tag{6}$$

where $\tau' = \frac{1}{\sqrt{3}} \cdot \frac{f_{sy} + f_{su}}{2}$; α_s is the ratio between the tangent modulus of the second stage and that of the first stage in the trilinear shear–deformation relationship and can be taken as 0.1 according to material testing results [7].

2.2 Shear capacity and deformation of concrete at panel zone

As in a 2D joint, the shear transfer mechanism of the concrete at the panel zone of a 3D joint can be described using the strut model [8]. In this paper, two mechanisms – the shear capacities of the main compression strut (V_{cu1}) and the additional confined compression strut (V_{cu2}) – contribute to the overall shear capacity of the concrete. For a joint under planar loading, the main compression strut and the additional confined compression strut are illustrated in Fig. 2(a) for loading in the XZ plane and in Fig. 2(b) for loading in the YZ plane. The corresponding shear–deformation relationship was already detailed in [5].

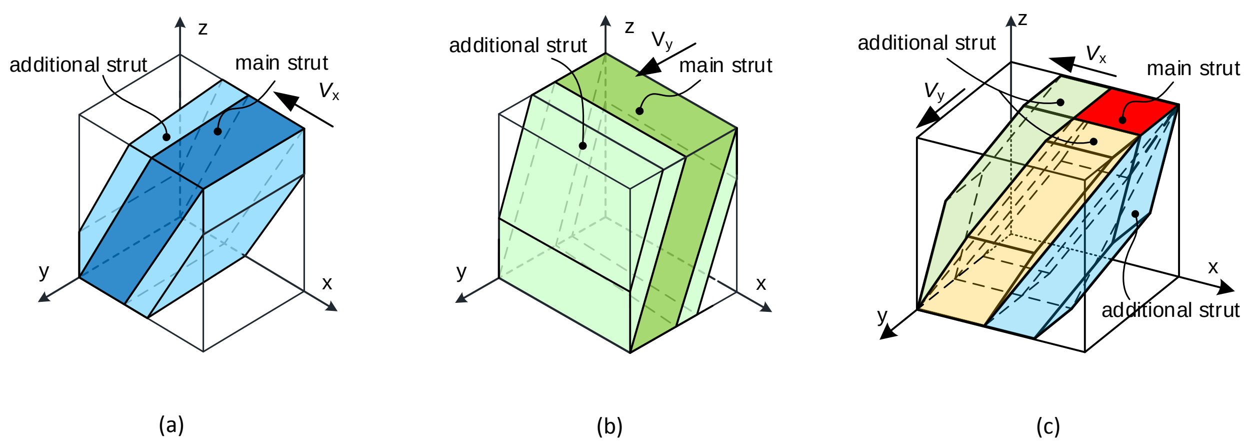

Fig. 2. Compression strut model for concrete at panel zone of a composite joint under loading in (a) XZ plane, (b) YZ plane and (c) 3D loading (bi-directional loading)

Moreover, with the loadings from two planes in a 3D joint, the main and additional compression struts as shown in Fig. 2(c) are in 3D stress states. Accordingly, their orientation, shape and size may differ from those in a planar loading state. According to theory developed for reinforced concrete, the shear capacity of the main compression strut is formed through an arch mechanism. The additional compression struts in a 3D composite joint (Fig. 2(c)) are further confined by the steel tube flange. The shapes and orientations of the main and additional struts in the 3D composite joint shown in Fig. 2(c) were obtained as a result of the superposition effect of the corresponding main and additional struts from the two planar loading scenarios (i.e. Fig. 2(a) and (b)). Hence the main strut in a 3D state is determined as the overlap of the two main struts from two planar loading states in Fig. 2(a) and (b).

To extend the modeling of concrete shear capacity of a 2D joint to a 3D configuration, the challenge is to take into account the 3D stress states of the main and additional compression struts. The subscripts “3D” and “2D” are used below to distinguish the variables (e.g. shear capacities) in 3D and planar loading states. The mechanism of the main compression strut in a 3D shear state is illustrated in Fig. 3. $V_{\text{cu1-3D}}$ is the shear capacity of the main strut and $\sigma_{\text{cb}} b^2 \cos\theta_{\text{3D}}$ is the corresponding axial force. θ_{3D} is the inclination angle of the main strut with respect to the concrete core (i.e. the angle between AC_1 and axis Z). Plane $C_1C_2C_3C_4$ presents a cross section cut from the main compression strut to form an isolated body for establishing the relationship between the shear capacity $V_{\text{cu1-3D}}$ and the axial force $\sigma_{\text{cb}} b^2 \cos\theta_{\text{3D}}$.

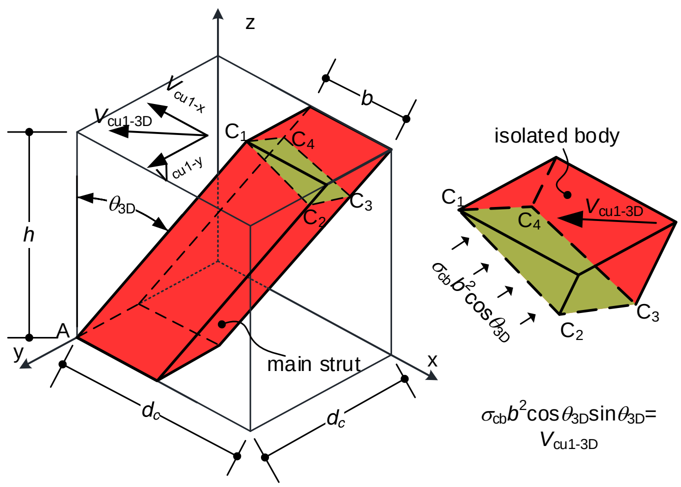

Fig. 3. Stress state of main compression strut mechanism of concrete in the panel zone of a 3D composite joint

Considering the force equilibrium in the horizontal direction of the isolated body (Fig. 3), the shear capacity of the main compression strut of concrete $V_{\text{cu1-3D}}$ can be established as:

$$V_{\text{cu1-3D}} = \sigma_{\text{cb}} b^2 \sin\theta_{\text{3D}} \cos\theta_{\text{3D}} \tag{7}$$

where σ_{cb} is the compression strength of the concrete; θ_{3D} is the inclination angle of the compression strut with respect to the square concrete core; b is a dimension parameter illustrated in Fig. 3 and is determined by geometric relation as:

$$b = d_{\text{c}} - \frac{\sqrt{2}}{2} h \tan\theta \tag{8}$$

where d_{c} and h are the width and the height respectively of the panel zone as illustrated in Fig. 3.

Substituting Eq. (8) into Eq. (7) gives:

$$V_{\text{cu1-3D}} = \sigma_{\text{cb}} d_{\text{c}}^2 (1 - \frac{\sqrt{2}}{2} \alpha \tan\theta_{\text{3D}})^2 \sin\theta_{\text{3D}} \cos\theta_{\text{3D}} \tag{9}$$

where α is the aspect ratio of the panel zone, $\alpha = h/d_{\text{c}}$

From Eq. (9) it can be seen that the inclination angle θ_{3D} should be determined first, in order to calculate the shear capacity of main compression strut ($V_{\text{cu1-3D}}$). Based on the lower bound theorem of classical plasticity theory [9], the stress state illustrated in Fig. 3 is a statically admissible field and the corresponding shear capacity is the lower bound of the true shear capacity. The maximum value of $V_{\text{cu1-3D}}$ with respect to θ_{3D} in Eq. (9) represents the closest estimation of the true shear capacity. Therefore, the inclination angle θ_{3D} can be determined when $V_{\text{cu1-3D}}$ reaches its maximum value in Eq. (9). To find the maximum point of $V_{\text{cu1-3D}}$, Eq. (9) is differentiated with respect to θ_{3D}. Eq. (10) can be obtained therefore:

$$\frac{\partial V_{\text{cu1-3D}}}{\partial \theta_{\text{3D}}} = \frac{\frac{\sqrt{2}}{2}\alpha \tan\theta_{\text{3D}} \text{-} 1}{\cos\theta_{\text{3D}}} \left[\left(\frac{\sqrt{2}}{2} \alpha \sin\theta_{\text{3D}} \text{-} \cos\theta_{\text{3D}} \right) \cos 2\theta_{\text{3D}} + \sqrt{2} \alpha \sin\theta_{\text{3D}} \right] = 0 \tag{10}$$

Eq. (10) is a nonlinear equation that determines the relationship between the aspect ratio α and inclination angle θ_{3D}. It is difficult to find the analytical solution of inclination angle θ_{3D} as a function of aspect ratio α. Matlab 2009b® was used to obtain a numerical solution for various values of aspect ratio α in the range of engineering practice ; then a simplified formulation for θ_{3D} as a function of α is obtained by data regression as:

$$\theta_{3D} = 0.468 \arctan\left(\frac{d_c}{h}\right) = 0.468 \arctan\left(\frac{1}{\alpha}\right) \tag{11}$$

The shear capacity of the main compression strut can then be rewritten as:

$$V_{cu1\text{-}3D} = \frac{1}{2}\sigma_{cb} b^2 \sin 2\theta_{3D} \tag{12}$$

where b and θ_{3D} are determined by Eqs. (8) and (11) respectively.

In a similar manner to the additional compression strut mechanism in a planar shear state [5], the additional compression struts in a 3D shear state are illustrated in Fig. 4. Four additional compression struts exist, as shown in Fig. 4 (with different colors), and they are confined by the flanges of the steel tube. Due to the interaction of the steel tube flange, two plastic hinges may be formed at the two ends of each additional compression strut.

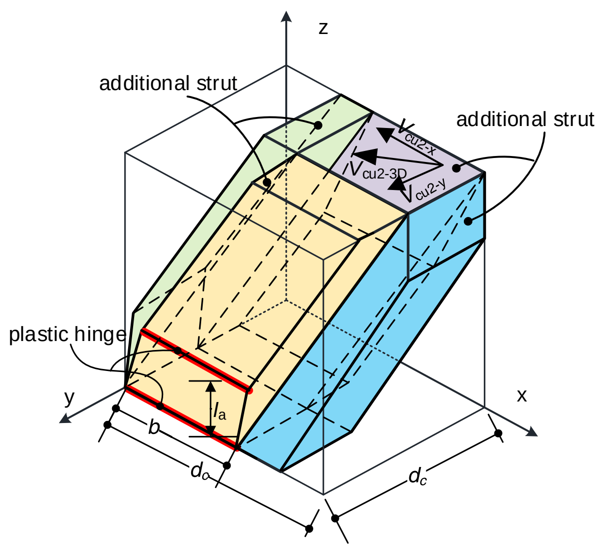

Fig. 4. Additional compression struts of concrete in the panel zone of a 3D joint

The formulation of the shear capacity $V_{cu2\text{-}3D}$ of one additional strut is derived as below, according to the mechanism illustrated in Fig. 5 (a) (b) (c). Because the x or y components of $V_{cu2\text{-}3D}$ are provided by two additional compression struts, the contribution of each additional strut to the overall shear capacity is obtained as $\sqrt{2}\, V_{cu2\text{-}3D}/4$.

$$V_{cu2\text{-}3D} = 4\sqrt{M_f b \sigma_{cb}} \sin\theta_{3D} \tag{13}$$

where M_f is the plastic moment capacity of the flange plate of the steel tube and can be expressed as:

$$M_f = \frac{1}{4} b t_s^2 f_{sy} \tag{14}$$

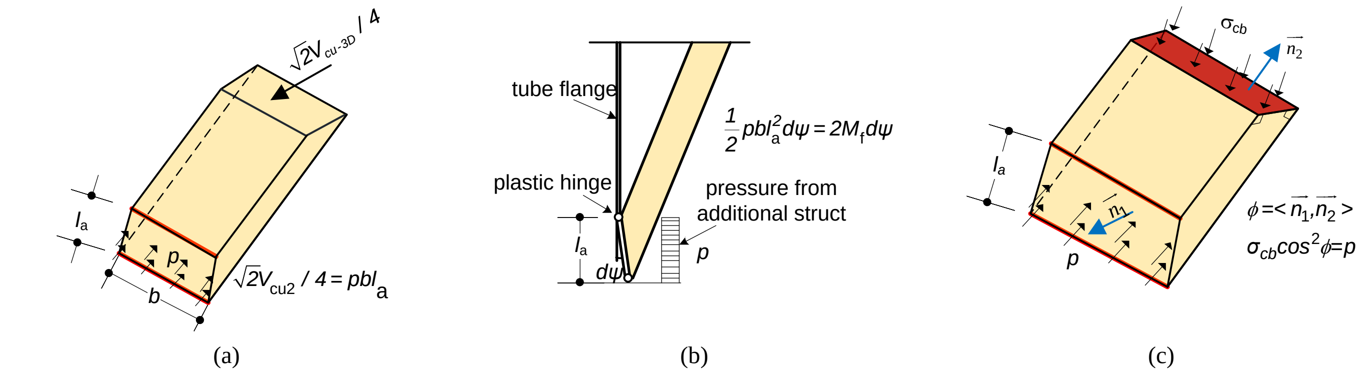

Fig. 5. Derivation of the shear capacity of the additional compression strut for a 3D joint (a) horizontal force equilibrium (b) ultimate limit state of steel flanges (c) axial force equilibrium of additional strut

Considering that shear capacity is often designed in the directions of the principal axes (x and y) of the two orthogonal beams, the shear capacity ($V_{\text{cu-x}}$ or $V_{\text{cu-y}}$) of the concrete in the panel zone of a 3D composite joint can be calculated in these two directions according to Eq. (15), which was derived based on Eqs. (12) and (13):

$$V_{\text{cu-x}} = \frac{\sqrt{2}}{2}\left(V_{\text{cu1-3D}} + V_{\text{cu2-3D}}\right) = \frac{\sqrt{2}}{2}\left(b\cos\theta_{\text{3D}} + 4\sqrt{\frac{M_{\text{f}}}{b\sigma_{\text{cb}}}}\right)b\sigma_{\text{cb}}\sin\theta_{\text{3D}} \tag{15}$$

The deformation at the ultimate shear strength of a 3D concrete core is given as [5]:

$$\gamma_{\text{cu-x}} = \kappa_{\text{c}}\frac{V_{\text{cu-x}}}{\alpha_{\text{cu}}A_{\text{c}}G_{\text{c}}} \tag{16}$$

where κ_{c} is the shear coefficient of the concrete core (1.2 for square concrete); G_{c} is the shear modulus of the concrete core; A_{c} is the cross-sectional area of the concrete core. α_{cu} is the stiffness reduction ratio as given by [5]:

$$\alpha_{\text{cu}} = 0.00158\sigma_{\text{cb}} + 0.0411\frac{h}{d_c} + 0.086 \tag{17}$$

where the compression strength of the concrete σ_{cb} is in units of MPa.

2.3 Shear capacity and deformation of a 3D composite joint

The total shear capacity $V_{\text{3D-x}}$ of a joint in a 3D loading state is the superposition of the shear capacity of the concrete core (Eq. (3)) and that of the steel webs (Eq. (15)):

$$V_{\text{3D-x}} = V_{\text{su}} + V_{\text{cu-x}} = \frac{\sqrt{2}}{2}\left(b\cos\theta_{\text{3D}} + 4\sqrt{\frac{M_{\text{f}}}{b\sigma_{\text{cb}}}}\right)b\sigma_{\text{cb}}\sin\theta_{\text{3D}} + \frac{A_{\text{w}}\sqrt{f_{\text{su}}^2 - \sigma_{\text{s}}^2}}{\sqrt{3}} \tag{18}$$

The shear–deformation relationship of a 3D composite joint may include four linear segments, as a result of the superposition of the trilinear model of the steel tube and the ideal elastoplastic model of encased concrete. For composite joints with fully developed shear strength and shear strain in the joint region, the webs of the steel tube usually yield first and then the concrete in the panel zone reaches its ultimate shear strain. Finally, the web of the steel tube reaches its ultimate state. The shear–deformation relationship is shown in Fig. 6, where point A corresponds to the yielding point of the panel zone; point B is determined by the shear deformation at which the concrete core just reaches the ultimate shear strength; and point C represents the ultimate shear strength of the panel zone corresponding to the ultimate state of the steel tube.

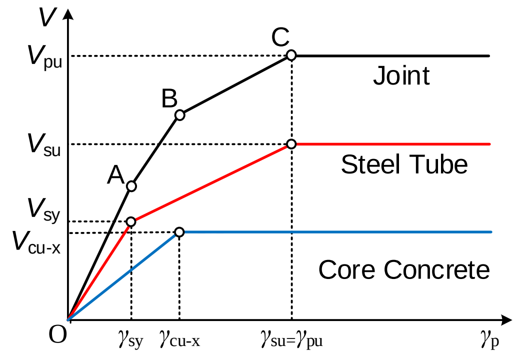

Fig. 6. Shear–deformation relationship with four linear segments for the panel zone

It is also important to evaluate the ratio of shear capacities in 3D and planar loading states ($V_{3D\text{-}x}/V_{2D}$). For such evaluation, a yield to tensile ratio (f_{su}/f_{sy}) of 1.3 and an axial compression ratio of 0.2 ($N_0/$ ($A_c\sigma_{cb}+A_sf_{sy}$), where N_0 is column axial force, A_c and A_s are section areas of concrete and steel tube respectively) are adopted to calculate the joint shear capacity $V_{3D\text{-}x}$ (Eq. (18)). Figs. 7 and 8 clearly illustrate the effects of the aspect ratio α, width to thickness ratio r_w (d_c/t_s) and strength ratio r_σ (f_{sy}/σ_{cb}) on the reduction of joint shear capacity subjected to loading from 2D to 3D. Again, the aspect ratio shows significant reduction in capacity.

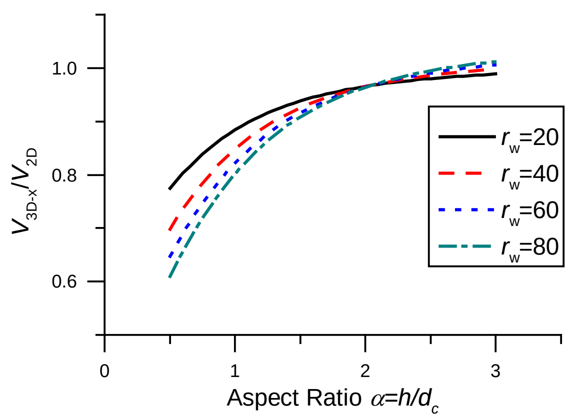

Fig. 7. Relationship between r_w and $V_{3D\text{-}x}/V_{2D}$ (r_σ=10)

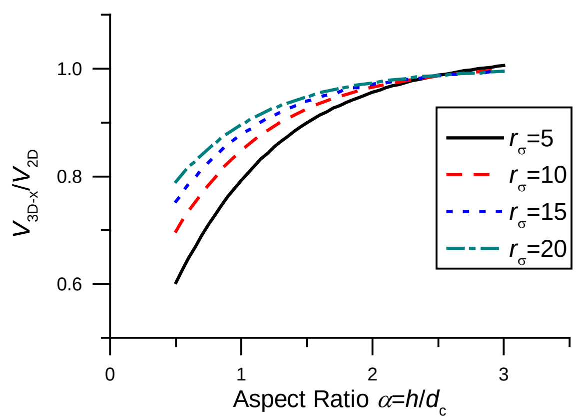

Fig. 8. Relationship between r_σ and $V_{3D\text{-}x}/V_{2D}$ (r_w=40)

Clearly, higher width to thickness ratios and lower strength ratios lead to more remarkable spatial coupling effects. The effects of the width to thickness ratio r_w and the strength ratio r_σ are more considerable on joint shear capacity with smaller aspect ratios. In the worst case (i.e., small aspect and strength ratios but a large width to thickness ratio), joint shear capacity in 3D loading may correspond to only 60% of that in 2D loading.

3 EXPERIMENTAL VALIDATION

To validate the analytical modeling developed above, four specimens (J101, J202, J203 and J301) were designed and tested under reversed-cyclic loading [7]. The specimens were CFT columns with steel beams through interior diaphragm connections. Specimen J202 was the reference specimen, the dimensions of which are shown in Fig. 9 in detail. The geometries of specimens J101 and J301 were the same as that of J202, but no concrete slab was placed on top of the steel beam for J101, and no encased concrete was placed in the steel tubular column (but with a different tube thickness of 12 mm) for J301. Specimen J203 had beams in only one plane and was tested under a uni-directional reversal loading whereas the other specimens had beams in two planes and were tested under bi-directional reversal loading. The experimental setup and loading configuration are shown in Fig. 10.

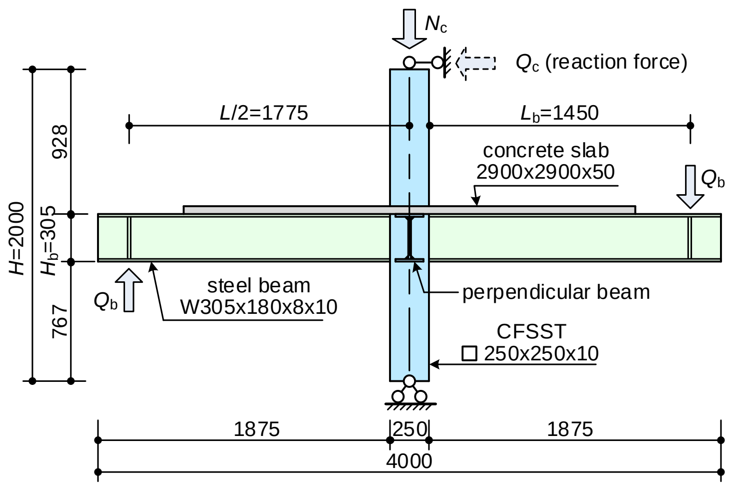

Fig. 9. Dimensions of the joint specimens (J202)

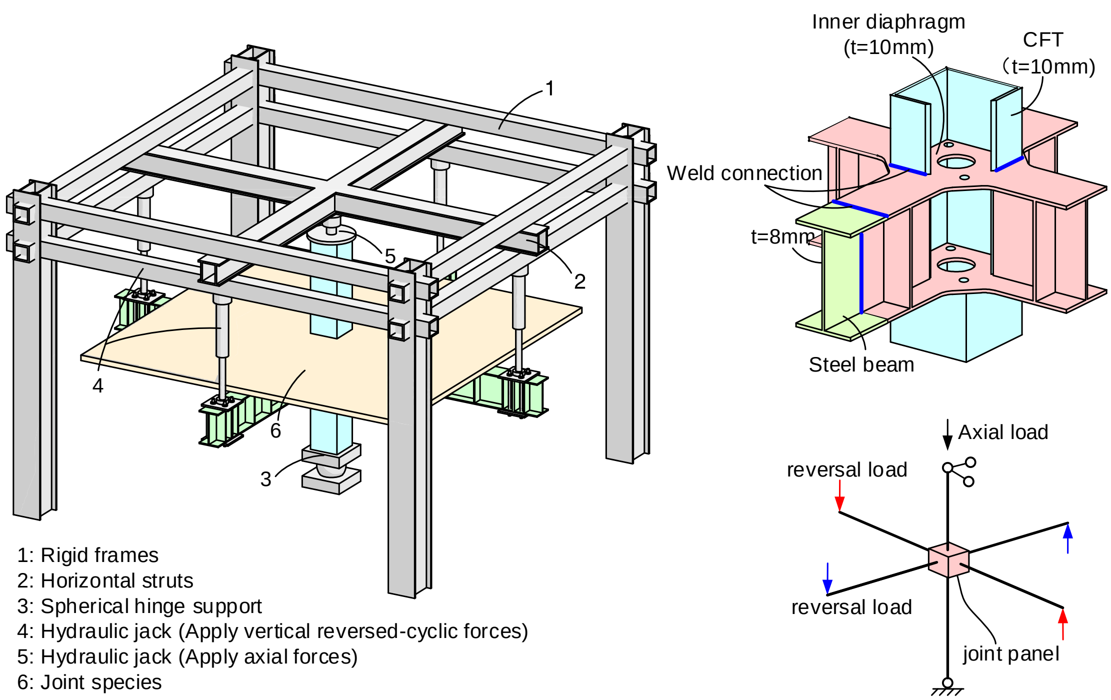

Fig. 10. Schematic diagram of experimental setup, joint details, and loading configuration for specimen J202

During the tests, a constant axial force was first applied on the top of the column as shown in Figs. 9. Vertical reversed-cyclic loads were applied at the ends of four beams (two beams in each plane), in a force control mode until the measured strains in the steel beam or steel panel exceeded the material yield strain, and subsequently in a displacement control mode.

The final failure mode of all four specimens was a typical shear failure in the panel zone of the joints, as shown in Fig. 11. The shear failures were characterized by fracture of the steel wall in the panel zone and crushing of the encased concrete within. These specimens therefore provide valuable information for examining the proposed analytical model developed for the joint shear capacity.

(a) (b) (c)

Fig. 11. Typical failure modes of the four specimens (a) fracture of steel tube (J101); (b) Crushing of encased concrete (J202) and (c) Overall deformation (J101)

The shear capacities of the specimens were calculated using the proposed formulation developed for 3D composite joints (Eq. (18)). The calculated values are compared with the experimental results in Table 1, where V_{su} and V_{cu} are the calculated contributions from the steel tube and the encased concrete according to Eqs. (3) and (15) respectively; V_{pu} is the total shear capacity of the 3D joint calculated by Eq. (18) and V_{eu} is the measured shear capacity of the joint from experiments.

Table 1. Comparison of predicted shear capacities with experimental results

No.	V_{su}/kN	V_{cu}/kN	V_{pu}/kN	V_{eu}/kN
J101	1336.0	284.0	1620.0	1743.7
J202	1336.0	275.4	1611.4	1594.8
J203	1336.0	457.2	1793.2	1944.0
R1	806.4	1579.6	2386.0	2384.6
R6	808.7	914.8	1723.5	1787.6

Overall, good agreement between the calculated (V_{pu}) and measured (V_{eu}) total shear capacities was found, with a maximum discrepancy less than 8%. Specimen J202 associated with beams in two planes was also compared to J203 with beams only in one plane. It was found that that the experimental result for the joint shear capacity of J202 was about 18% lower than that of J203, and 11% lower than the predicted shear capacity of J203. This comparison indicates that using the planar shear formulation may overestimate the joint shear capacity in the case of a 3D loading configuration and this may lead to unsafety.

Further, joint shear–deformation curves were formed by the calculated shear capacity values and the corresponding shear deformation for specimen J202 and J203, as shown in Fig. 12. The highly nonlinear experimental shear–deformation skeleton curve can be relatively well described by the proposed modeling curve with four linear segments. Discrepancies between the experimental and predicted shear–deformation skeleton curves were mainly found at the second and third segments between the yield and ultimate states. These discrepancies may resulted from the assumption of an ideal elastoplastic shear–deformation relationship of the concrete core.

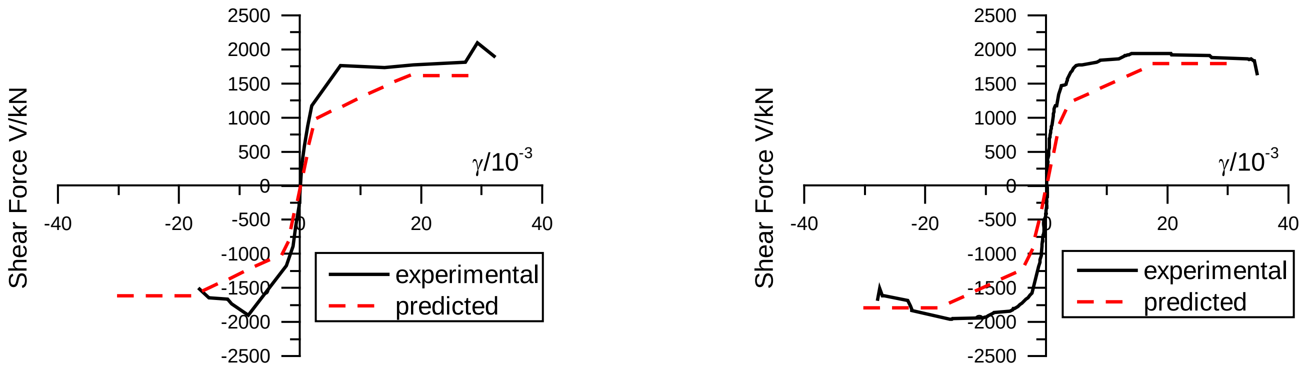

(a) (b)

Fig. 12. Comparison of experimental and predicted skeleton curves of specimen (a) J202 (bi-directional loading) and (b) J203 (uni-directional loading)

The 3D shear capacity model was further validated by the experimental results reported in [4]. The specimens R1 and R6 were tested under uni-directional and bi-directional reversal loading respectively, and were similar to specimens J202 and J101. The predicted and experimental results are compared in the last two rows in Table 1 and good agreement is evident, with discrepancies less than 5%. The planar shear capacity of specimen R6 was calculated as 2222.6 kN by the equations introduced by [4] and this value was 24% higher than the experimental result (1787.6 kN, see Table 1). It is evident for specimen R6 that the spatial coupling effect significantly weakened the shear capacity of the joint subjected to 3D loading. This is because in this case, high-strength concrete (σ_{cb}=97.7 MPa) was used for specimen R6, leading to a rather small steel to concrete strength ratio ($r_{\sigma}=f_{sy}/\sigma_{cb}$=5.0).

4 CONCLUSIONS

An analytical model was developed in this paper to estimate the shear capacity of 3D composite joints of CFT columns and steel beams subjected to shear forces in two planes. In this model, the main compression strut and additional compression strut mechanisms were formulated for the concrete core of the joint panel subjected to 3D loading scenario. The joint shear capacity was calculated and compared with experimental results where the specimens were subjected to reversed-cyclic loading in two planes and failed through shear mode at the joints. The joint shear–deformation relationship was characterized by a piecewise linear model with four segments, taking into consideration the effects of shear forces in two planes. The modeling results of joint shear capacities and shear–deformation relationships were validated by the experimental results from references. Based on this work, the following conclusions can be drawn:

1) The analytical model developed in this paper suggests that 3D (bi-directional) loading weakens the shear capacity of the concrete panel zone, although it does not affect the shear capacity of the webs of the steel tube. Because of the loadings from two planes and the associated space coupling effects on a 3D joint, the main and additional compression struts, obtained as a result of superposition of two 2D joints in the corresponding plane loading state, may present different orientations, shapes and sizes from those in a planar loading state.

2) A new piecewise linear constitutive model based on the superposition principle was implemented into the shear–deformation relationship of 3D composite joints. This constitutive model was characterized by the analytic ultimate shear strength formula in 3D shearing states, and therefore the spatial coupling effect caused by bi-directional shear to the concrete zone could be taken into consideration. The predicted and experimental shear–deformation curves showed satisfactory agreement. The major discrepancy was found between yield and ultimate states because of the assumption of an ideal elastoplastic shear–deformation relationship of the concrete core.

3) The proposed model for the shear capacity of composite joints of CFT columns was validated by the results from 2D and 3D joint experiments. Further calculations also indicated that using the planar shear capacity formulation for a joint in a 3D shear state may lead to an overestimation of 10%~20% for the joint shear capacity. The reduction in joint shear capacity due to a 3D loading configuration depends mainly on the aspect ratio of the joint panel, the steel to

concrete strength ratio and the width to thickness ratio of the steel tube. A decrease in the aspect ratio results in the most notable reduction in joint shear capacity and such a reduction also becomes more considerable with an increase in the width to thickness ratio or a decrease in the strength ratio. For a worst-case scenario where the joint has a relatively small aspect ratio (0.5 for example), a large width to thickness ratio (80.0 for example) and a small strength ratio (5.0 for example), joint shear capacity in the 3D shear state can reduce to only 60% of that in the 2D loading state.

Acknowledgement

The authors appreciate the financial support of the National Natural Science Foundation of China (No. 51222810) and the Specialized Research Fund for the Doctoral Program of Higher Education of China (No. 20120002110003).

References

[1] Koester BD (2000): Panel zone behavior of moment connections between rectangular concrete-filled steel tubes and wide flange beams. University of Texas at Austin.

[2] Cheng CT, Chung LL (2003): Seismic performance of steel beams to concrete-filled steel tubular column connections Journal of Constructional Steel Research 59:405-426.

[3] Cheng CT, Chan CF, Chung LL (2007): Seismic behavior of steel beams and CFT column moment-resisting connections with floor slabs Journal of Constructional Steel Research 63:1479-1493.

[4] Nishiyama I, Fujimoto T, Fukumoto T, Yoshioka K (2004): Inelastic force-deformation response of joint shear panels in beam-column moment connections to concrete-filled tubes Journal of Structural Engineering 130:244-252.

[5] Fukumoto T, Morita K (2005): Elastoplastic behavior of panel zone in steel beam-to-concrete filled steel tube column moment connections Journal of structural engineering 131:1841-1853.

[6] Architectural Institute of Japan (AIJ) (1987): AIJ standard for structural calculation of steel reinforced concrete structures. Tokyo, Japan.

[7] Fan J, Li Q, Nie J, Zhou H: Experimental Study on the Seismic Performance of 3D Joints between Concrete-Filled Square Steel Tubular Columns and Composite Beams. Journal of Structural Engineering 2014; 140(12): 114-121.

[8] Paulay T, Park R, Preistley MJN (1978): Reinforced concrete beam-column joints under seismic actions. In: ACI Journal Proceedings.

[9] Chen W-F (2013): Limit analysis and soil plasticity. Elsevier.

[10] Nie JG, Qin K, Cai CS (2008): Seismic behavior of connections composed of CFSSTCs and steel–concrete composite beams—finite element analysis Journal of Constructional Steel Research 64:680-688.